International Scholarly Research Network
ISRN Ceramics
Volume 2011, Article ID 406094, 8 pages
doi:10.5402/2011/406094

Research Article

Microstructure, Mössbauer, and Optical Characterizations of Nanocrystalline α-Fe_2O_3 Synthesized by Chemical Route

Abhijit Banerjee,[1] Soumitra Patra,[1] Mahuya Chakrabarti,[2] Dirtha Sanyal,[3] Mrinal Pal,[4] and Swapan Kumar Pradhan[1]

[1] *Department of Physics, University of Burdwan, Golapbag, Burdwan 713104, India*
[2] *Department of Physics, University of Calcutta, 92 Acharya Prafulla Chandra Road, Kolkata 700009, India*
[3] *Variable Energy Cyclotron Centre, 1/AF, Bidhannagar, Kolkata 700064, India*
[4] *Central Mechanical Engineering Research Institute, Durgapur 713209, India*

Correspondence should be addressed to Swapan Kumar Pradhan, skp_bu@yahoo.com

Received 9 June 2011; Accepted 10 July 2011

Academic Editors: V. Fruth, H. Maiwa, W.-C. Oh, and W. Tseng

Nanocrystalline α-Fe_2O_3 of crystallite sizes ranging from 18 nm to 54 nm has been prepared by sol gel process and postannealing the powder up to 500°C. X-ray diffraction and transmission electron microscopy images have been used for determining the average crystallite sizes of the prepared samples. The Rietveld analysis reveals that the "as-prepared" α-Fe_2O_3 powders are not completely stoichiometric, and significant (~20%) oxygen vacancies are noticed in the α-Fe_2O_3 lattice. Oxygen atoms in as-prepared sample are significantly displaced and the lattice is heavily distorted. With increasing annealing temperature the lattice approaches towards the stoichiometric oxygen concentration and perfect lattice configuration. Mössbauer spectrum of the unannealed (as-prepared) α-Fe_2O_3 sample shows the superparamagnetic behavior at room temperature whereas all annealed samples show complete ferromagnetic behavior. Optical band gaps of these nanocrystalline α-Fe_2O_3 samples have been measured from UV-Vis spectroscopy and found to decrease from 2.65 eV to 2.50 eV, like an n-type semiconductor, with increasing annealing temperature up to 500°C.

1. Introduction

Nanostructured materials (oxides) nowadays attract lots of attention as their structure and properties can be manipulated by changing the surface to volume ratio [1], preparation process [2], annealing temperature [3], and by changing the crystallite size [4]. Properties of the nanomaterials can also be controlled by incorporating different types of defects inside nanocrystals [5]. Nanocrystalline magnetic metal oxides have received special attention as they can be used in different fields, for example, magnetic resonance imaging [6], drug delivery agents [7], and so forth. Further, an unusual characteristic like superparamagnetism [8] in nanocrystalline state of these materials makes them object of great interest for fundamental studies.

Among different magnetic nanoparticles, α-Fe_2O_3 is a very common magnetic material as it has potential applications in chemical industry [9]. It can be used as catalyst, gas sensing material to detect combustible gases [10] like CH_4 and C_3H_8, and so forth. Among different iron oxides, α-Fe_2O_3 is the most stable polymorph in nature under ambient condition and can be easily found as mineral hematite. Hematite has a rhombohedrally centered hexagonal structure of the corundum type with a close-packed oxygen lattice in which two-thirds of the octahedral sited are occupied by Fe (III) ions [11].

Nanocrystalline α-Fe_2O_3 powders have been prepared by different preparation techniques like sol-gel [12], hydrothermal [13], chemical vapor phase deposition [14], calcinations of hydroxides [15], radio frequency sputtering [16], gas condensation technique [17], and high-energy ball-milling process [18, 19]. Kündig et al. [20] measured the Mössbauer spectra of Fe^{57} in α-Fe_2O_3 as a function of particle size and temperature and noticed that bulk α-Fe_2O_3 changed

in the sign of the quadrupole interaction in going through the Morin transition temperature, 263 K. They reported the superparamagnetic behavior of α-Fe_2O_3 when the particle size is less than 13 nm and as the particle size gradually increased, it became ferromagnetic. Giri et al. [21] prepared single-phased α-Fe_2O_3 nanoparticles using a hydrothermal synthesis method in aqueous-organic microemulsion under mild alkaline condition. They confirmed the uniformity of nanocrystalline α-Fe_2O_3 particles both by XRD and HRTEM studies and obtained sextet pattern for these crystallites from the Mössbauer study. Lemine et al. [22] studied the effect of high-energy ball milling on α-Fe_2O_3 particles and characterized the ball-milled powders by the Rietveld analysis based on XRD patterns and Mössbauer spectroscopy and revealed that the magnetic hyperfine field was affected by the grain size. Sahu et al. [23] noticed the phase transformation reaction in nanocrystalline α-Fe_2O_3 powder induced by ball milling under both air and oxygen atmospheres. They revealed that the transformation of α-Fe_2O_3 to Fe_3O_4 and finally to FeO occurs in both atmospheres depending upon the oxygen partial pressures. In none of the above cases, detailed microstructure characterization and oxygen vacancies in α-Fe_2O_3 lattice have been estimated by the Rietveld method of structure refinement, and magnetic structures have been corroborated to the microstructure parameters and oxygen vacancies. The purposes of the present work are to (i) establish a correlation in between microstructure parameters and oxygen vacancies with magnetic properties of nanocrystalline α-Fe_2O_3 and postannealed powders and (ii) estimate the optical band gaps of nanocrystalline α-Fe_2O_3 under the influence of lattice distortion. Optical band gaps of as-prepared and postannealed samples have been measured by the UV-Vis absorption spectroscopic method. Goyel et al. [24] measured the direct band gap 2.5 eV of nanocrystalline Fe_2O_3 powder synthesized by modified CVD technique. Fu et al. [25] reported that the α-Fe_2O_3 nanoparticles exhibited n-type semiconducting (SC) properties under ambient conditions with a band gap of 2.2 eV. Sahana et al. [26] reported that the band gap for α-Fe_2O_3 nanoparticle was 2.3 eV, and bandgap increases by the decreasing size of Fe_2O_3 crystallites which was manifested in terms of the quantum confinement effect.

2. Experimental Outline

In the present study, reagent grade $Fe(NO_3)_3$, $9H_2O$ has been used as precursor for the preparation of nanocrystalline α-Fe_2O_3 powder by chemical route. Initially, a solution of $Fe(NO_3)_3$, $9H_2O$ is made with distilled water. A few drops of concentrated nitric acid have been added to keep the pH level of the solution in acidic range. This solution is then stirred for 1 h and then poured into a plastic flat-bottomed container and left for three days in ambient atmosphere for gelation. The gel is then evaporated to obtain "as-prepared" sample in powder form [27]. The dry powder is then annealed in open air at different temperatures, 300°C, 350°C, and 500°C for 1 h in a precisely controlled furnace.

The X-ray powder diffraction data of as-prepared and annealed samples have been recorded in a Philips PW 1830 X-ray powder diffractometer using Ni-filtered CuK_α radiation. In each case, step-scan data have been obtained in the 20°–80° 2θ in a step size of 0.02° and 5 sec/step counting time. All experimental patterns are fitted very well and the structure and microstructure parameters like crystallite size, lattice parameters, oxygen concentration, and displacement of oxygen atoms in α-Fe_2O_3 lattice are obtained from the Rietveld analysis [22–26].

Transmission electron microscopy with TECNAI S-TWIN (FEI Company) electron microscope operating at 200 kV has been used to estimate the average crystallite size of different nanocrystalline α-Fe_2O_3 samples. A pinch of powder was ultrasonically dispersed in alcohol, and a drop of the solution was put on a 300 mesh copper grid for the transmission electron microscopy work.

Room temperature ^{57}Fe Mössbauer spectra for all samples have been recorded in the transmission configuration with constant acceleration mode. A gas filled proportional counter has been used for the detection of 14.4 keV Mössbauer γ-rays, while a 10 mCi ^{57}Co isotope embedded in an Rh matrix has been used as the Mössbauer source. The Mössbauer spectrometer has been calibrated with 95.16% enriched $^{57}Fe_2O_3$ and standard α-^{57}Fe foil. The Mössbauer spectra have been analyzed by a standard least square fitting program (NMOSFIT).

The UV-Vis absorption spectra of all samples have been recorded in a Hitachi U-3501 spectrophotometer in the wavelength range 200–800 nm.

3. Method of Microstructure Analysis by Rietveld Refinement

In the present study, we have adopted the Rietveld's powder structure refinement analysis [28–33] of X-ray powder diffraction data to obtain the refined structural parameters, such as atomic coordinates, occupancies, lattice parameters, thermal parameters, and so forth, and microstructure parameters, such as crystallite size and r.m.s. lattice strain. The Rietveld's software MAUD 2.06 [31] is specially designed to refine simultaneously both the structural and microstructure parameters through least-squares method. The instrumental broadening for the present experimental setup has been obtained using a specially prepared Si-standard, free from all kinds of lattice imperfections. The peak shape is assumed to be a pseudo-Voigt (pV) function with asymmetry because it takes individual care for both the crystallite size and strain broadening of the experimental profiles. The background of each pattern is fitted by a polynomial function of degree 4. The theoretical X-ray powder diffraction pattern is simulated containing all structure and a trial set of microstructure parameters of rhombohedral α-Fe_2O_3 phase. A detailed mathematical description of the Rietveld analysis has been reported elsewhere [28–31]. Considering the integrated intensity of the peaks as a function of structural and microstructure parameters, the Marquardt least-squares procedures are adopted for the minimization of the difference between the observed and simulated powder diffraction patterns and the minimization was monitored

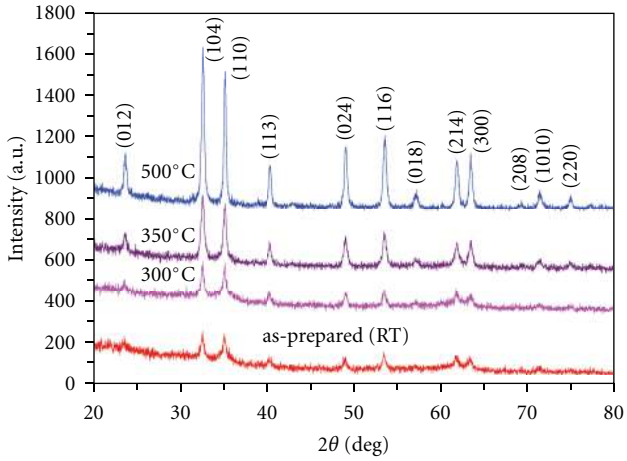

Figure 1: X-ray powder diffraction patterns for different α- Fe_2O_3 sample.

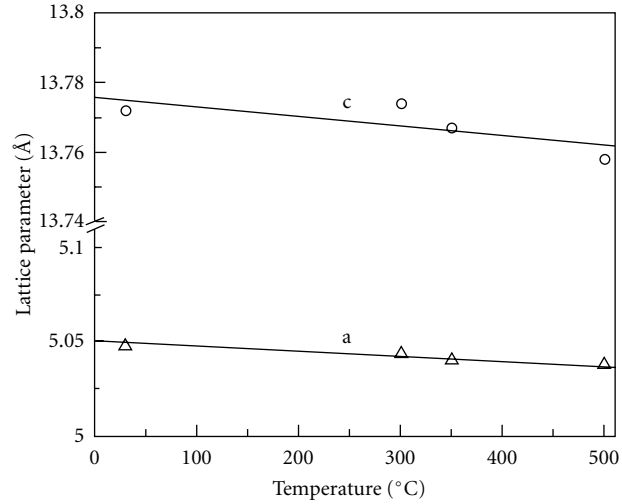

Figure 2: Variation of lattice parameter with temperature of α-Fe_2O_3 samples.

using the reliability index parameters, R_{wp} (weighted residual error), and R_{exp} (expected error) defined respectively as

$$R_{wp} = \left[\frac{\sum_i w_i(I_0 - I_c)^2}{\sum_i w_i(I_0)^2}\right]^{1/2},$$
$$R_{exp} = \left[\frac{(N-P)}{\sum_i w_i(I_0)^2}\right]^{1/2}, \quad (1)$$

where I_0 and I_c are the experimental and calculated intensities, $w_i(= I/I_0)$ and N are the weight and number of experimental observations, and P the number of fitting parameters. This leads to the value of goodness of fit (GoF) [28–31]

$$\text{GoF} = \frac{R_{wp}}{R_{exp}}. \quad (2)$$

Refinement continues till convergence is reached with the value of the quality factor, GoF very close to 1 (varies between 1.1 and 1.7), which confirms the goodness of refinement.

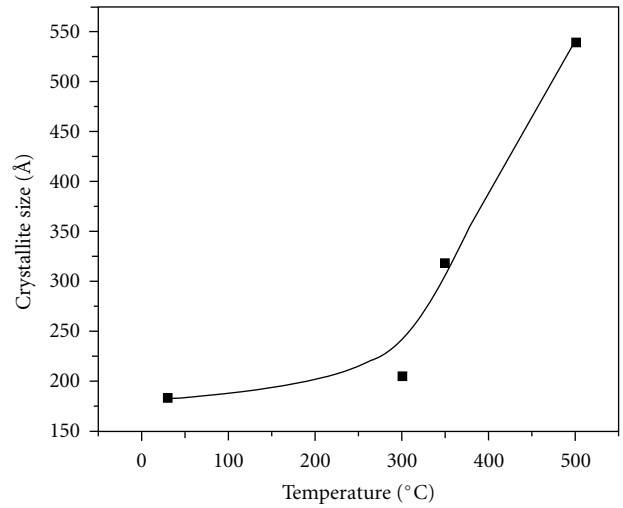

Figure 3: Variation of crystallite size of α-Fe_2O_3 samples with temperature.

4. Results and Discussion

4.1. Microstructure Characterization Using XRD and HRTEM. The nanocrystalline α-Fe_2O_3 powder is prepared from the ferric-nitrate solution and then annealed at 300°C, 350°C, and 500°C in open air. Figure 1 shows the X-ray powder diffraction patterns of these samples. It is evident from the figure that all strong α-Fe_2O_3 reflections appear clearly in the XRD pattern of as-prepared sample with significant peak-broadening. The peak broadening reduces, and intensity of all reflections increases continuously with increasing annealing temperature up to 500°C. The intensity ratios of all reflections agree well with the reported pattern (JCPDS File # 33-0664, Space group: R3-cH (hexagonal setting)). For microstructure characterization of these samples, the Rietveld structure and microstructure refinement method has been adopted in the present study, and all experimental data are fitted with the simulated XRD patterns containing only the α-Fe_2O_3 phase. All experimental patterns are fitted very well and the structure and microstructure parameters are obtained from the Rietveld analysis. Both the "a" and "c" lattice parameters of α-Fe_2O_3 lattice are significantly large in "as-prepared" sample than the reported values (a = 5.0356 Å, c =13.7489 Å) [34] and decrease continuously (Figure 2) towards the reported values with increasing annealing temperature up to 500°C. It signifies that the lattice of the "as prepared" sample contains a significant amount of lattice strain and almost strain-free α-Fe_2O_3 lattice is obtained after annealing the powder at 500°C for 1 hr.

Considering all reflections the Rietveld analysis reveals that the shape of α-Fe_2O_3 crystallites is isotropic in nature and their size variation with increasing annealing temperature is shown in Figure 3. The crystallite size of the "as-prepared" powder is ~18 nm and remains almost unchanged

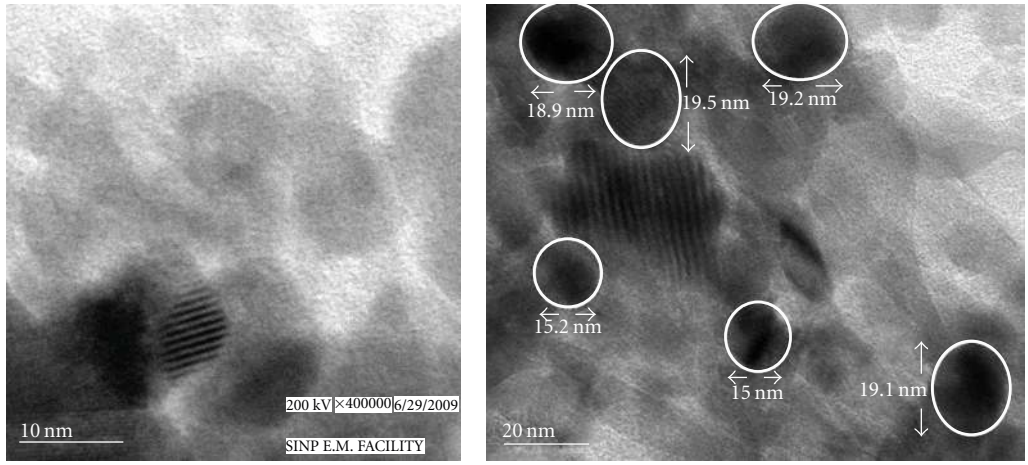

(a) (b)

Figure 4: HRTEM image of α-Fe_2O_3 crystallites in unannealed (as-prepared) sample. (b) HRTEM image of α-Fe_2O_3 crystallites in 300°C annealed sample.

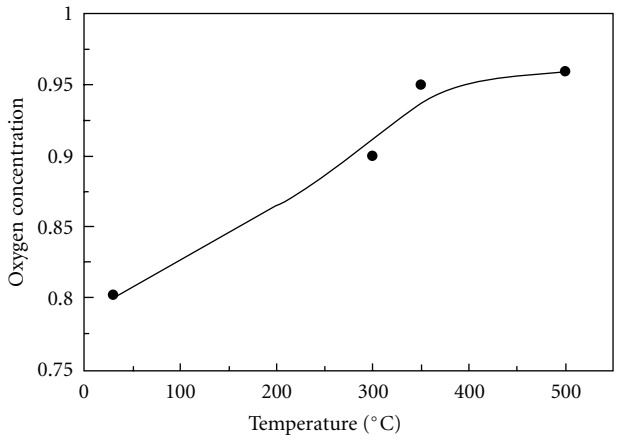

Figure 5: Variation of oxygen concentration with temperature.

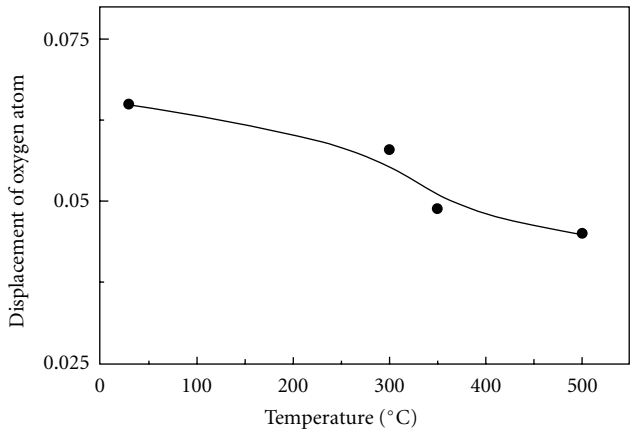

Figure 6: Variation of displacement of oxygen with temperature.

up to 300°C and then increases sharply to ~54 nm after annealing the powder at 500°C for 1 h. Figures 4(a) and 4(b) depict the HRTEM image of as-prepared powder sample. It is evident from the image that particles are almost spherical in shape, and average particle size is ~18 nm which is very close to that obtained from X-ray analysis. The as-prepared lattice is highly strained which is clearly evidenced by the presence of Moire fringe in the HRTEM image.

The Rietveld analysis reveals that the "as-prepared" α-Fe_2O_3 powder is not completely stoichiometric, and there are significant amount of oxygen vacancies present in the α-Fe_2O_3 lattice and oxygen atoms are displaced from their stable position. The variation of oxygen concentration with increasing annealing temperature is shown in Figure 5. In as-prepared lattice, ~20 mol% oxygen positions remain unoccupied and with increasing annealing temperature, most of the positions are occupied and the lattice approaches towards the stoichiometric oxygen concentration and after annealing at 500°C, it becomes saturated and only 4 mol% oxygen positions remain unfilled. It seems that all oxygen positions in α-Fe_2O_3 powder may not be completely filled up even after annealing the powder sample at higher temperatures. From the analysis it is also revealed that the displaced oxygen atoms in the nonstoichiometric "as-prepared" sample (z = 0.29) approach towards their normal positions (z = 0.32) as in the bulk α-Fe_2O_3 (ICSD Code No. 82904) (Figure 6). These observations indicate that the nonstoichiometric and heavily distorted as-prepared α-Fe_2O_3 lattice approaches gradually towards stoichiometric and perfect lattice configuration with increasing annealing temperature.

4.2. Magnetic Characterization Using Mössbauer Spectroscopy. Figures 7(a) and 7(b) show the room temperature Mössbauer spectra for the as-prepared and 350°C annealed samples, respectively. It is clear from these figures that the as-prepared sample shows a doublet type of Mössbauer spectra, and no ferromagnetic nature (six line pattern of Mössbauer spectra) has been observed. This clearly indicates that the as-prepared

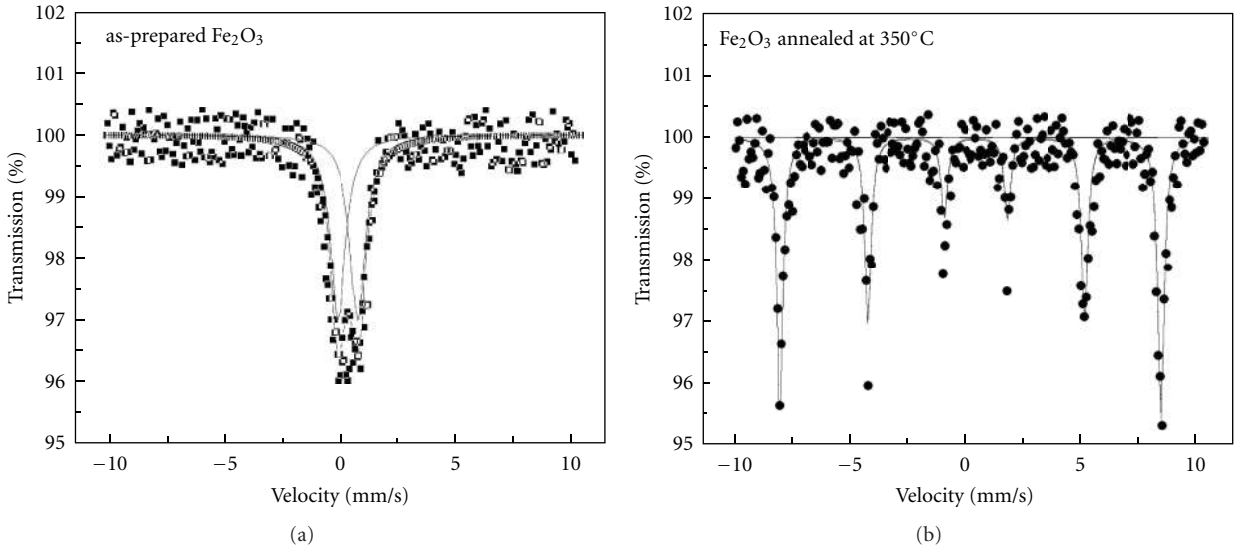

Figure 7: (a) Room temperature Mössbauer spectrum for annealed α-Fe_2O_3 sample. (b) Room temperature Mössbauer spectrum for the "as-prepared" α-Fe_2O_3 sample.

Table 1: Values of the Mössbauer parameters, IS, QS, and HF for the "as-prepared" and 500°C annealed Fe_2O_3 samples.

Sample	IS (mm/sec)	Line width (mm/sec)	HF (Tesla)	QS (mm/sec)
Nanocrystalline Fe_2O_3	0.42	10.41 ± 0.482	—	0.7934
500°C annealed Fe_2O_3	0.36	3.95 ± 0.23	78.8	−0.1250

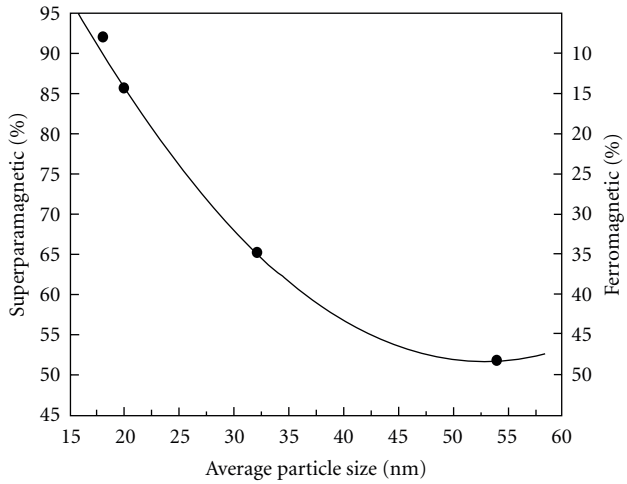

Figure 8: Variation of ratio of superparamagnetic fraction of α-Fe_2O_3 particles to the ferromagnetic fraction with the crystallite size.

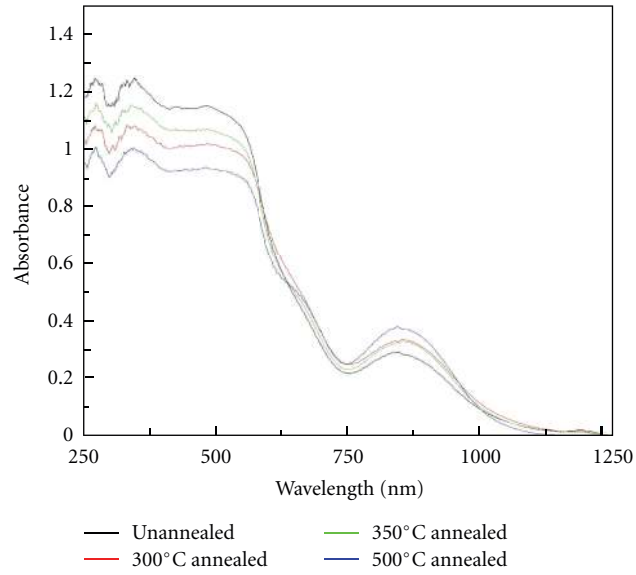

Figure 9: UV-Vis absorption spectra for different α-Fe_2O_3 samples.

α-Fe_2O_3 powder is superparamagnetic in nature. The 350°C annealed sample and all other annealed samples (300°C and 500°C) show sextet patterns in Mössbauer spectra confirming the appearance of ferromagnetic nature in these annealed samples. From the experimental Mössbauer spectra both isomer shift (IS), quadrupole splitting (QS), and hyperfine field (HF) have been calculated by a standard least-square fitting program, NMOSFIT. Values of the IS, QS, and HF for as-prepared and 500°C annealed samples are summarized in Table 1.

From Table 1 it has been observed that the nanocrystalline as-prepared sample shows enhanced IS, line width, and QS values in comparison to the annealed sample. In the as-prepared sample there are two components. The first one is the grain consisting of all atoms located in the lattice

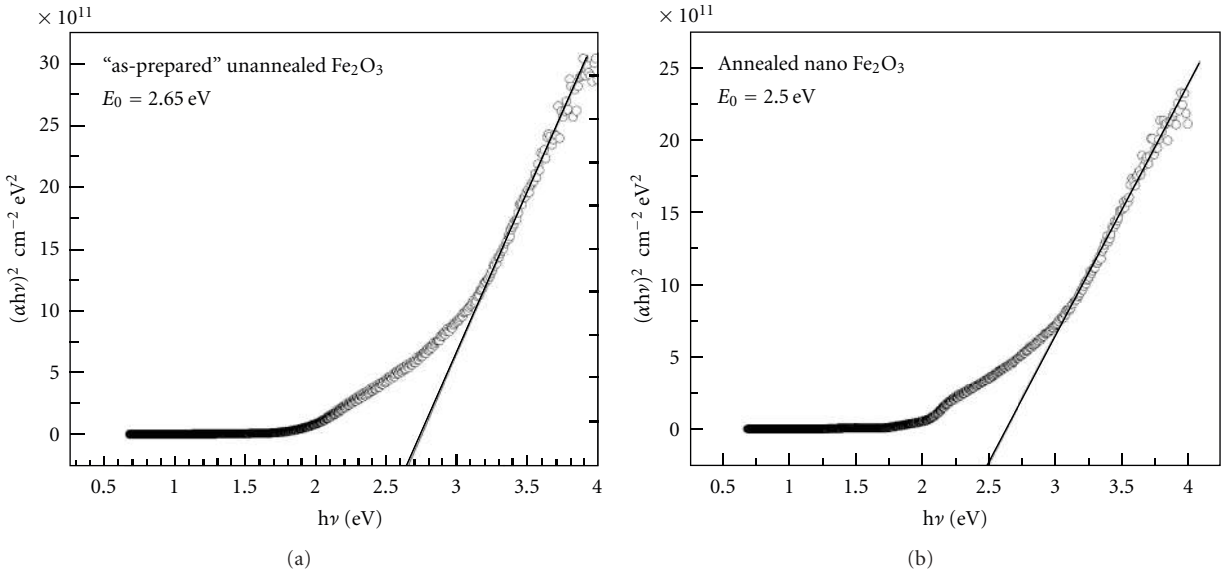

Figure 10: (a) Band gap estimation for unannealed (as-prepared) sample. (b) Band gap estimation for annealed sample.

of the crystallites, and the second one is the interfacial component consisting of all the atoms situated in the grain boundaries of the crystallites. The enhanced IS, line width, and QS for the as-prepared sample may be due to the reduction of the electron density at the interfacial site in presence of lattice imperfections. The HF value for the 350°C annealed sample is also higher than that of the standard α-Fe_2O_3 sample (52 T). This enhanced HF value may be due to the low electron density at the interfacial site in this annealed sample compared to the bulk standard α-Fe_2O_3 sample. From the Rietveld analysis it has been shown that the oxygen concentration increases gradually with annealing temperature, and displaced oxygen atoms approach towards their equilibrium positions during annealing. It suggests that the as-prepared distorted lattice contains significant amount of lattice imperfections, and the enhancement in all magnetic parameters may be attributed to the high density of point defects in the as-prepared sample.

Figure 8 represents the variation of ratio of superparamagnetic fraction of α-Fe_2O_3 particles to the ferromagnetic fraction with increasing crystallite size. This fraction has been calculated by directly integrating the absorptions lines. It indicates that both superparamagnetism and ferromagnetism persist in these nanoparticles. From Mössbauer spectroscopy measurements It has been reported earlier [22] that there are two kinds of particles which coexist in the sample: nanostructured and micrometric hematite. Nanostructured particles result in superparamagnetism, and relatively bigger particles having less lattice imperfections are responsible for ferromagnetism. This nature of change in magnetic behaviour with change in particle size is already noticed by several researchers [20–22, 24–26]. It is evident from the variation that superparamagnetism in as-prepared sample caused mainly due to lattice imperfections in α-Fe_2O_3 lattice for the following possible reasons. (i) Oxygen vacancy in the lattice reduces the Fe-O dipoles; (ii) displacement of oxygen atoms from their equivalent positions enhances the Fe-O bond lengths; (ii) magnetic dipoles are randomly oriented in presence of lattice imperfections.

4.3. Optical Characterization Using UV-Vis Spectroscopy. Optical band gaps of as-prepared and all annealed samples have been measured using UV-Vis absorption spectroscopic technique. The spectral absorption coefficient, α, is defined as [35]

$$\alpha(\lambda) = \frac{4\pi k(\lambda)}{\lambda}, \tag{3}$$

where $k(\lambda)$ is the spectral extinction coefficient obtained from the absorption curve and λ is the wavelength. Figure 9 represents the absorbance curve for as-prepared and all annealed samples. It is clearly observed that the absorption maxima occur around ~475 nm for all the samples. Thus the position of the absorption maxima remains almost the same for the nanocrystalline as-prepared and the annealed samples. The band gap, E_g (for a direct transition between the valence and conduction band), is obtained by fitting the experimental absorption data with the following equation:

$$(\alpha h\nu)^2 = A\left(h\nu - E_g\right), \tag{4}$$

for a direct band gap transition, [35] where $h\nu$ is the photon energy, α is the absorption coefficient, E_g is the band gap, and A is a characteristic parameter independent of photon energy. Figures 10(a) and 10(b) represent the absorption curves of as-prepared and 500°C annealed powders for direct transition. The value of band gap E_g (for direct transition) has been obtained from the intercept of the extrapolated linear part of the $(\alpha h\nu)^2$ versus $h\nu$ curve with the energy ($h\nu$) axis. The band gap for direct transition (estimated from Figures 10(a) and 10(b)) for the as-prepared nanocrystalline sample is 2.65 eV at the wavelength 468 nm, whereas for

the annealed sample the value reduces to 2.50 eV. Thus the as-prepared and annealed α-Fe_2O_3 nanoparticles are n-type semiconductor which was already noticed earlier [24–26] and there is a red shift in the band gap with annealing of the samples.

5. Conclusion

Nanocrystalline α-Fe_2O_3 crystallites of size ranging 18 to 54 nm have been prepared by chemical synthesis. The Rietveld analysis reveals that the "as-prepared" α-Fe_2O_3 powders is not completely stoichiometric, and significant oxygen vacancies are noticed in the α-Fe_2O_3 lattice. With increasing annealing temperature the lattice approaches towards the stoichiometric oxygen concentration. The "as-prepared" sample shows superparamagnetic behavior at the Mössbauer spectra whereas the annealed samples show both superparamagnetic and ferromagnetic behaviors. From Mössbauer spectra it has been observed that the nanocrystalline as-prepared sample shows enhanced IS, line width, and QS values compared to the annealed samples which may be due to the reduction of the electron density at the interfacial site. From UV-Vis absorption spectra it has been observed that the band gaps of the annealed samples are lower than the as-prepared samples and all samples belong to n-type semiconductors.

Acknowledgment

One of the authors (M. Chakrabarti) is gratefully acknowledges UGC, Government of India for providing financial assistance as *Dr. Kothari postdoctoral fellowship*. SP is grateful to UGC, Government of India for providing financial assistance in the form of a fellowship.

References

[1] A. Henglein, "Small-particle research: physicochemical properties of extremely small colloidal metal and semiconductor particles," *Chemical Reviews*, vol. 89, no. 8, pp. 1861–1873, 1989.

[2] J. Drbohlavova, R. Hrdy, V. Adam, R. Kizek, O. Schneeweiss, and J. Hubalek, "Preparation and properties of various magnetic nanoparticles," *Sensors*, vol. 9, no. 4, pp. 2352–2362, 2009.

[3] S. Volden, A. L. Kjøniksen, K. Zhu, J. Genzer, B. Nyström, and W. R. Glomm, "Temperature-dependent optical properties of gold nanoparticles coated with a charged diblock copolymer and an uncharged triblock copolymer," *ACS Nano*, vol. 4, no. 2, pp. 1187–1201, 2010.

[4] M. Chakrabarti, S. Dutta, S. Chattapadhyay, A. Sarkar, D. Sanyal, and A. Chakrabarti, "Grain size dependence of optical properties and positron annihilation parameters in Bi_2O_3 powder," *Nanotechnology*, vol. 15, no. 12, pp. 1792–1796, 2004.

[5] M. Chakrabarti, A. Banerjee, D. Sanyal, M. Sutradhar, and A. Chakrabarti, "Particle size dependence of optical and defect parameters in mechanically milled Fe_2O_3," *Journal of Materials Science*, vol. 43, no. 12, pp. 4175–4181, 2008.

[6] H. Basti, L. Ben Tahar, L. S. Smiri et al., "Catechol derivatives-coated Fe_3O_4 and γ-Fe_2O_3 nanoparticles as potential MRI contrast agents," *Journal of Colloid and Interface Science*, vol. 341, no. 2, pp. 248–254, 2010.

[7] K. A. Hinds, J. M. Hill, E. M. Shapiro et al., "Highly efficient endosomal labeling of progenitor and stem cells with large magnetic particles allows magnetic resonance imaging of single cells," *Blood*, vol. 102, no. 3, pp. 867–872, 2003.

[8] D. H. Jones, "Mössbauer spectroscopy and the physics of superparamagnetism," *Hyperfine Interactions*, vol. 47-48, no. 1-4, pp. 289–297, 1989.

[9] N. Mimura, I. Takahara, M. Saito, T. Hattori, K. Ohkuma, and M. Ando, "Dehydrogenation of ethylbenzene over iron oxide-based catalyst in the presence of carbon dioxide," *Catalysis Today*, vol. 45, no. 1-4, pp. 61–64, 1998.

[10] L. Huo, W. Li, L. Lu et al., "Preparation, structure, and properties of three-dimensional ordered α-Fe_2O_3 nanoparticulate film," *Chemistry of Materials*, vol. 12, no. 3, pp. 790–794, 2000.

[11] R. Zboril, M. Mashlan, and D. Petridis, "Iron(III) oxides from thermal processes-synthesis, structural and magnetic properties, Mössbauer spectroscopy characterization, and applications," *Chemistry of Materials*, vol. 14, no. 3, pp. 969–982, 2002.

[12] R. Pascual, M. Sayer, C. V. R. V. Kumar, and L. Zou, "Rapid thermal processing of zirconia thin films produced by the sol-gel method," *Journal of Applied Physics*, vol. 70, no. 4, pp. 2348–2352, 1991.

[13] X. Wang, X. Chen, X. Ma, H. Zheng, M. Ji, and Z. Zhang, "Low-temperature synthesis of α-Fe_2O_3 nanoparticles with a closed cage structure," *Chemical Physics Letters*, vol. 384, no. 4-6, pp. 391–393, 2004.

[14] E. T. Kim and S. G. Yoon, "Characterization of zirconium dioxide film formed by plasma enhanced metal-organic chemical vapor deposition," *Thin Solid Films*, vol. 227, no. 1, pp. 7–12, 1993.

[15] X. Bokhimi, A. Morales, M. Portilla, and A. García-Ruiz, "Hydroxides as precursors of nanocrystalline oxides," *Nanostructured Materials*, vol. 12, no. 1, pp. 589–592, 1999.

[16] W. G. Luo, A. L. Ding, X. T. Chen, and H. Li, "Preparation and properties of nano-crystalline $Pb_{0.72}La_{0.28}TiO_3$ thin films," *Integrated Ferroelectrics*, vol. 9, pp. 75–80, 1995.

[17] R. Birringer, H. Gleiter, H. P. Klein, and P. Marquardt, "Nanocrystalline materials an approach to a novel solid structure with gas-like disorder?" *Physics Letters A*, vol. 102, no. 8, pp. 365–369, 1984.

[18] D. Michel, E. Gaffet, and P. Berthet, "Structure of nanosized refractory oxde powders," *Nanostructured Materials*, vol. 6, no. 5–8, pp. 667–670, 1995.

[19] M. Chakrabarti, D. Bhowmick, A. Sarkar et al., "Doppler broadening measurements of the electron-positron annihilation radiation in nanocrystalline ZrO_2," *Journal of Materials Science*, vol. 40, no. 19, pp. 5265–5268, 2005.

[20] W. Kündig, H. Bömmel, G. Constabaris, and R. H. Lindquist, "Some properties of supported small α-Fe_2O_3 particles determined with the mössbauer effect," *Physical Review*, vol. 142, no. 2, pp. 327–333, 1966.

[21] S. Giri, S. Samanta, S. Maji, S. Ganguli, and A. Bhaumik, "Magnetic properties of α-Fe_2O_3 nanoparticle synthesized by a new hydrothermal method," *Journal of Magnetism and Magnetic Materials*, vol. 285, no. 1-2, pp. 296–302, 2005.

[22] O. M. Lemine, M. Sajieddine, M. Bououdina, R. Msalam, S. Mufti, and A. Alyamani, "Rietveld analysis and Mössbauer spectroscopy studies of nanocrystalline hematite α-Fe_2O_3," *Journal of Alloys and Compounds*, vol. 502, no. 2, pp. 279–282, 2010.

[23] P. Sahu, M. De, and M. Zdujić, "Microstructural characterization of the evoluted phases of ball-milled α-Fe_2O_3 powder in air and oxygen atmosphere by Rietveld analysis," *Materials Chemistry and Physics*, vol. 82, no. 3, pp. 864–876, 2003.

[24] R. N. Goyal, A. K. Pandey, D. Kaur, and A. Kumar, "Fabrication of α-Fe_2O_3 nanopowder modified glassy carbon electrode for applications in electrochemical sensing," *Journal of Nanoscience and Nanotechnology*, vol. 9, no. 8, pp. 4692–4699, 2009.

[25] X. Fu, F. Bei, X. Wang, X. Yang, and L. Lu, "Surface-enhanced Raman scattering of 4-mercaptopyridine on sub-monolayers of α-Fe_2O_3 nanocrystals (sphere, spindle, cube)," *Journal of Raman Spectroscopy*, vol. 40, no. 9, pp. 1290–1295, 2009.

[26] M. B. Sahana, C. Sudakar, G. Setzler et al., "Bandgap engineering by tuning particle size and crystallinity of SnO_2-Fe_2O_3 nanocrystalline composite thin films," *Applied Physics Letters*, vol. 93, no. 23, Article ID 231909, 2008.

[27] A. E. Gash, T. M. Tillotson, J. H. Satcher, J. F. Poco, L. W. Hrubesh, and R. L. Simpson, "Use of epoxides in the sol-gel synthesis of porous iron(III) oxide monoliths from Fe(III) salts," *Chemistry of Materials*, vol. 13, no. 3, pp. 999–1007, 2001.

[28] H. M. Rietveld, "Line profiles of neutron powder diffraction peaks for structure refinement," *Acta Crystallographica*, vol. 22, pp. 151–152, 1967.

[29] H. M. Rietveld, "A profile refinement method for nuclear and magnetic structures," *Journal of Applied Crystallography*, vol. 2, pp. 65–71, 1969.

[30] R. A. Young and D. B. Willes, "Profile shape functions in Rietveld refinements," *Journal of Applied Crystallography*, vol. 15, pp. 430–438, 1982.

[31] L. Lutterotti, "Maud Version 2.14," 2009, http://www.ing.unitn.it/~Luttero/maud.

[32] B. Ghosh and S. K. Pradhan, "Microstructure characterization of nanocrystalline Fe3C synthesized by high-energy ball milling," *Journal of Alloys and Compounds*, vol. 477, no. 1-2, pp. 127–132, 2009.

[33] S. Patra, B. Satpati, and S. K. Pradhan, "Microstructure characterization of mechanically synthesized ZnS quantum dots," *Journal of Applied Physics*, vol. 106, no. 3, Article ID 034313, 2009.

[34] S. Dutta, S. Chattopadhyay, A. Sarkar, M. Chakrabarti, D. Sanyal, and D. Jana, "Role of defects in tailoring structural, electrical and optical properties of ZnO," *Progress in Materials Science*, vol. 54, no. 1, pp. 89–136, 2009.

[35] J. Tauc, "Absorption edge and internal electric fields in amorphous semiconductors," *Materials Research Bulletin*, vol. 5, no. 8, pp. 721–729, 1970.